Reference: *Biol. Bull.* **194:** 304–316. (June, 1998)

Oyster Shell Protein and Atomic Force Microscopy of Oyster Shell Folia

C. S. SIKES[1,*], A. P. WHEELER[2], A. WIERZBICKI[3], R. M. DILLAMAN[4], AND L. DE LUCA[2]

[1] *The Mineralization Center, Department of Biological Sciences, and* [3] *Department of Chemistry, University of South Alabama, Mobile, Alabama 36688;* [2] *Department of Biological Sciences, Clemson University, Clemson, South Carolina 29634-1903; and* [4] *Department of Biological Sciences, University of North Carolina at Wilmington, Wilmington, North Carolina 28403-3297*

Abstract. The organic layers within biominerals often are viewed as sheets that may function in part to limit and define the underlying crystal structure, as well as to promote formation of the next mineral layer. Some insights into the nature of the sheets were revealed by atomic force microscopy (AFM) of surfaces of freshly cleaved fragments of oyster shell folia. Visible in the micrographs were arrays of globular structures that resembled the globules seen in isolated oyster shell protein bound to calcite, mica, and glass. The results of chemical treatment showed that the foliar globules slowly dissolved in 5.25% NaOCl or 1 *N* NaOH, reacted with an antibody prepared against an isolated oyster shell protein, and were hydrolyzed by several proteolytic enzymes. These morphological and chemical observations suggested that protein was a significant component of the foliar globules. Although they might also have a significant mineral content, the foliar globules were not effective as nucleators of $CaCO_3$ crystal formation at low levels of supersaturation in artificial seawater. Overall, the results suggested that molecules of oyster shell protein may agglomerate and combine with mineral to form a surface of complex topography that coats the calcite laths but exhibits no obvious correspondence to any specific crystallographic plane.

Introduction

Information about the organization of shell and regulation of its growth is not only central to biomineralogy but also has increasingly attracted the attention of materials scientists (Wheeler and Koskan, 1993; Mann, 1996; Stupp and Braun, 1997; Weiner and Addadi, 1997). For example, there is interest in nanoscale approaches to making composite materials that have increased durability, elevated resistance to fracture, and other desirable properties. In shell, such properties are thought to be derived from the interplay of the mineral phases with the organic layers; the latter are viewed mainly as sheets that may nucleate the original crystal phase, then regulate and limit its growth so that a specific morphology results.

The organic and inorganic phases of the carbonate biominerals that occur in shells are well suited to atomic-level imaging by atomic force microscopy (AFM), as shown by a number of studies that probed the hard, flat mineral surfaces (Friedbacher *et al.*, 1991; Hilner *et al.*, 1992; Drake *et al.*, 1992; Donachy *et al.*, 1992; Sikes *et al.*, 1993). There also have been AFM observations of protein molecules isolated from calcite oyster shell, as well as of peptide analogs of the protein, bound to specific surfaces of calcite (Wierzbicki *et al.*, 1994; Sikes and Wierzbicki, 1995a, b). The isolated oyster shell protein had an ellipsoid, globular appearance when attached to calcite grown *in vitro* and viewed by AFM.

The polygonal crystalline arrays of aragonite from molluscan nacre also have been studied by AFM (Giles *et al.*, 1994, 1995; Manne *et al.*, 1994). The emphasis in these studies was on bleached biominerals, which thus were presumably free of the associated proteins. Although logically interpreted as composed of mineral only, many globules were observed that at least resembled the globules of isolated matrix proteins that we had reported, as

Received 30 April 1997; accepted 6 March 1998.

* To whom correspondence should be addressed. E-mail: ssikes@usamail.usouthal.edu

mentioned above. Along these lines, Gutmannsbauer and Hanni (1994) viewed nacreous tablets by a variety of techniques and interpreted both the X-ray reflections and the AFM images as showing an ordered layer of organic globules that coats each tablet. Shell organic layers have also been described in detail in many electron microscopy studies over the years.

For example, Watabe and coworkers studied transmission electron micrographs of Formvar replicas taken from the whole, inner surface of oyster shell (1958), Formvar replicas of fracture surfaces of oyster shell (1961), and diamond-knife sections of pieces of foliar layers of oyster shell with and without a decalcification treatment (1965), usually with silicon monoxide or carbon coatings. The images revealed distinct relationships between the organic and inorganic layers, in some cases including the presence of organic layers at the fracture surfaces. Although the spatial resolution of the surface topography was necessarily affected by the limitations of electron microscopy, especially when replicated and coated specimens were examined, the clarity of the images was nonetheless excellent, making possible the detection of globular and "reticular" structures on the foliar surfaces. Assignments of spatial dimensions of organic layers were made only of cross-sections and not of surface views; the assignments were based on the relative electron density of the layers. By this approach, the width of the proteinaceous layer between adjacent folia was estimated to be 12 to 20 nm.

Similarly, Taylor *et al.* (1969) and Carriker and coworkers (1979, 1980) used transmission and scanning electron microscopy (SEM) of coated replicas, diamond-wheel sections, and fracture surfaces in monographic studies of oyster shell ultrastructure. Many high-resolution images of all layers of the shell were produced. The large inner layer of calcite sheets, or folia, was one area of emphasis. Spatial relationships again were evident between the organic and inorganic constituents, with the observations and interpretations consistent with earlier studies. In a number of the images, globules are apparent on the surfaces of the folia, but no particular attention was drawn to them.

Previously, we reported AFM images of folia from the inner layer of oyster shell. Foliar chips, which are produced in abundance when a shell is cracked open, evidently cleave mainly along the interfaces where the proteins occur rather than through the mineral itself, and therefore might be coated with protein (Watabe, 1965; Taylor *et al.*, 1969; Carriker and Palmer, 1979; Carriker *et al.*, 1980; Kuhn-Spearing *et al.*, 1996). We had observed that the foliar surface contained globular ellipsoids resembling the globules of isolated oyster shell protein imaged both in fluids and dry on calcite, glass, and mica (Sikes and Wierzbicki, 1995a, b; 1996). Moreover, the foliar globules were susceptible to enzymatic hydrolysis (Sikes *et al.*, 1997).

The purpose of the present investigation was to establish the identity of the foliar globules more clearly as proteinaceous, mineral, or perhaps a combination of both. Approaches included chemical, enzymatic, and immunologic treatments together with AFM and SEM observations. In addition, the possible function of the foliar globules and their relationship to the adjacent mineral phases was investigated by AFM and SEM studies of nucleation of calcite on foliar chips. The results suggested that the proteinaceous layer of oyster shell folia is itself a composite of undefined mineral and agglomerations of individual protein molecules, which together form a layer of complex topography, rather than a linearized sheet, that overlies the calcite laths. As nucleators of crystal growth, the foliar globules were less effective than the areas of exposed calcite that may occur on the foliar surfaces. No obvious relationship of the foliar globules to specific crystallographic planes was found, although several possibilities were considered.

Materials and Methods

Oyster shell folia

The outer surface of freshly shucked shells of the American oyster, *Crassostrea virginica*, was ground using a hand-held Dremel to remove residual periostracum and outer prismatica. The shell was then fractured with a hammer. White, pearlescent foliated chips were separated from pigmented and chalky chips and stored dry in a vial. The chips were several millimeters in linear dimensions; they typically weighed between 20 and 30 mg, and did not exceed 100 mg.

Chemical treatments

Foliar chips were incubated in 10 ml of 1 *N* NaOH or 5.25% NaOCl (Clorox) in a glass vial for 3 weeks. The solution was changed daily. At intervals, a chip was removed with forceps, placed on a glass-fiber filter, and washed under gentle vacuum with 10 ml of 0.1 m*M* NaOH. Next, the chip was soaked for 10 min, 3 times, in 10 ml of an aqueous solution saturated with respect to calcite. This solution was the supernatant of a slurry of reagent-grade calcite crystal, 25 g/liter of water, stirred for 3 weeks. The chip then was placed on a piece of absorbent paper, air-dried for 1 h, and glued to a 12-mm glass disc by gently placing it on 10 μl of 3:1 dichloromethane and commercial polyurethane (Minwax), just after the dichloromethane had mostly evaporated, leaving a flat, nonwicking adhesive surface. This produced a firm,

insoluble attachment to the glass disc, which had been previously attached with superglue (cyanoacrylate) to an electron-microscopy stub. Epoxy was also acceptable for adhering the chips to glass, but superglue was not because it dissolved during aqueous imaging.

Control chips were incubated in calcite-saturated water and washed as above prior to viewing. They also were imaged directly, with no treatment, to ensure that the soaking and washing did not affect the control morphology. Some chips and control crystals of calcite also were rinsed in distilled water rather than calcite-saturated water. This had no effect on the overall appearance of the folia, but did etch the surface of the control crystals. Therefore, for AFM imaging at the atomic level, the calcite-saturated solution was preferable for rinsing. However, if the saturated solution was not quickly absorbed into the paper, the samples would occasionally exhibit ectopic crystals that formed from drying droplets.

Enzymatic treatments

Foliar chips were incubated for 48 h in 0.5 ml of phosphate buffer (0.05 *M*, pH 7.5) that contained 1.95 units of carboxypeptidase B (Sigma), 2 units of endoproteinase glu-C (Boehringer-Mannheim), or 1.5 units of subtilisin (Boehringer-Mannheim). Carboxypeptidase is a general protease of peptide bonds at the C-terminus. Endoproteinase glu-C and subtilisin both cleave internal peptide bonds, particularly of acidic residues, which are common in the oyster shell protein.

The chips were rinsed with distilled water and air dried prior to gluing onto the glass disc and AFM stub. Control chips were incubated in buffer alone.

Immunohistochemical treatments

An ELISA assay was performed directly on foliar chips, using an antibody prepared against a 48-kD protein band obtained by SDS-PAGE of whole, soluble protein extracts of folia (Myers *et al.*, 1996). The electroeluted protein was mixed 1:2 with Freunds incomplete adjuvant and injected intramuscularly (three injections) into single-comb white leghorn hens to stimulate antibody production. Approximately 2 weeks after the final injection, IgG was chloroform-extracted from egg yolks and purified by ethanol precipitation (after Mohammed *et al.*, 1986). Standard ELISA confirmed the reactivity of the extracted antibody with the 48-kD antigen and demonstrated cross-reactivity of the antibody with other isolated oyster shell matrix proteins (Johnstone and Wheeler, unpubl. data). The antibody did not react with β-lactoglobulin or BSA, which served as negative controls.

Foliar chips were incubated for 1 h in 1% BSA to block nonspecific binding, washed in two changes of TBS (Tris-buffered saline, pH 7.4), and then transferred to a 1:200 solution of the soluble matrix primary antibody. After 1 h, the chips were washed twice with TBS and transferred for 1 h to a 1:1200 solution of horseradish-peroxidase-conjugated goat anti-chicken secondary antibody (Sigma). After a final TBS wash, the DAB system (Sigma) was used to detect antibody binding to the foliar chips. Additional blocked (BSA-incubated) and unblocked (no BSA incubation) chips, incubated with secondary antibody only and developed using the DAB system, confirmed that there was very little nonspecific binding of the secondary antibody to the foliar shell.

Matched foliar chips were pretreated for 24 h with 1 ml of 0.1 *M* NaOH or 0.08 *M* EDTA solution (pH about 9.0) and then assayed as above. The EDTA solution was prepared so as to dissolve no more than 10% of the 80 mg of foliar shell. These treatments yielded ELISA results that were nearly as dark as those for untreated chips, indicating that most sites for primary antibody binding were still available. The slightly diminished reactivity of the treated chips suggested that some binding sites had been altered or removed via dissolution of protein or shell.

Foliar chips to be imaged by AFM were incubated in primary antibody only.

Atomic force microscopy

Constant-force, contact-mode AFM (Nanoscope III, Digital Instruments) was used to image foliar chips, both dry and in calcite-saturated artificial seawater (ASW: again, the supernatant of a slurry of calcite crystals as above, but prepared in 0.5 *M* NaCl, 0.011 *M* KCl, pH 8.3). Tapping-mode AFM was not needed for foliar images because the imaged surfaces and adsorbates were firm and stationary to contact-mode AFM. However, tapping-mode images were obtained for the various treatments and, in all cases, revealed morphologies similar to those obtained by contact mode. The images reported herein were all obtained by contact-mode AFM. Standard tips of Si_3N_4 were used for contact mode and tips of etched silica for tapping mode (both from Digital Instruments). The tip forces in contact mode were minimized at $\sim 10^{-9}$ N; however, the samples were stable under higher forces as well. The AFM scanner was adapted for use of SEM stubs.

Procedures to guard against artifacts included variation of the scan angle to make sure that the image rotated accordingly. In addition, for contact-mode imaging, tips were first used to obtain an atomic image of mica to be sure that the tip was performing optimally before imaging a sample. This procedure was repeated after an imaging session, as well as during a session if questionable features began to appear, to confirm that the tip was still

capable of producing images at the angstrom level. Tips that would not generate an atomic pattern of mica were discarded.

Morphology at the micrometer level as seen by AFM was corroborated by direct comparison of AFM and SEM images of similar surfaces. This was more satisfactory than use of several commercial and shareware deconvolution programs to remove any tip-related features from AFM images. These programs often yielded images of oyster shell folia or fields of randomly oriented crystals of calcite that conflicted with images of the same materials viewed by SEM.

AFM crystal growth assay

Metastable and spontaneously nucleating solutions of calcite-supersaturated ASW were gently pumped through a fluid cell (Digital Instruments, volume ~150 μl) by use of a peristaltic pump (Cole-Parmer) at a flow rate of ~150 μl/min. The calcium concentration was 10 m*M*, with total dissolved inorganic carbon (DIC) varied from 2 to 10 m*M*. The solutions were first prepared in a three-necked, 50-ml round-bottom flask by addition of 30 ml of ASW, with smooth magnetic stirring. To this was added 0.3 ml of 1.0 *M* $CaCl_2 \cdot 2H_2O$, followed by appropriate volumes of 0.5 *M* $NaHCO_3$. The pH was adjusted to 8.30 with microliter amounts of 1 *N* NaOH and monitored by pH electrode and meter (Fisher 911) equipped with a strip chart (Cole-Parmer). The apparatus was not thermostated, but room temperature was recorded at 23° ± 2°C. At the initiation of the experiment, the fluid from the flask was pumped through the flow-cell of the AFM. The foliar chip was already in place and being imaged in calcite-saturated ASW.

In separate experiments, the metastability of the fluids was demonstrated by growth of 15 mg of $CaCO_3$ seeds, added to the flask as 1.5 ml of a 10 mg/ml seed suspension in saturated ASW. The primary stock of calcite seeds was prepared by stirring 100 g of reagent-grade calcite (Baker) in 1 l of ASW for at least 3 weeks (Wheeler *et al.*, 1991). In the absence of seed crystals, at 2 to 5 m*M* DIC, the solutions exhibited no spontaneous crystal formation over periods of at least 2 h of most imaging sessions. However, these solutions were shown to be supersaturated and were defined as metastable because crystal growth did occur in the presence of seed crystals. The growth was observed as a downward drift in pH resulting from incorporation of CO_3^{2-} ions into the seed-crystal lattice.

At a concentration of 7 m*M* DIC at pH 8.3, the calcite crystals did spontaneously nucleate after an induction period of 15 to 20 min. At concentrations of DIC higher than 7 m*M*, the induction of crystal growth, again monitored by downward pH drift, became increasingly more rapid, making real-time monitoring by AFM more difficult. In addition to rapid crystal formation over large regions of the foliar chip, the turbid suspension of calcite crystals at these concentrations of DIC interfered with the laser signal of the AFM.

Scanning electron microscopy

Foliar chips were dehydrated by vacuum at 1 mTorr for 15 min, then coated with a layer of approximately 20 nm of gold palladium in a Polaron sputter coater. Specimens were viewed with an ISI SX40 scanning electron microscope operated at 30 kV.

Results

Atomic force micrographs of dry, control, untreated foliar chips of oyster shell are shown in Figures 1, 3, 5, and 6. The folia are composed of individual crystalline laths lying side-by-side to form a sheet. Laths are typically about 2 μm in width, with lath heights in the imaged areas varying from 150 to 350 nm. Figures 1 and 3 are comparable in magnification to Figures 2 and 4, which are scanning electron micrographs of control, untreated foliar chips. Both Figures 1 and 2 are low magnifications that show the arrays of folia revealed by the fracturing process. Figures 3 and 4 show individual folia and reveal randomly broken ends, straight foliar margins, and a granular surface texture. Figures 5 and 6 are higher magnification AFM images that resolve the surface texture, identified in the lower magnification images from both SEM and AFM, into a continuous layer of discrete globules. These foliar globules typically were about 10 to 15 nm in height, but ranged up to about 40 nm.

The susceptibility of the foliar globules to dissolution in 1 *N* NaOH is shown in Figure 7. The foliar globules were seen to be relatively resistant to the NaOH treatment at 5 days. However, by 10 days (not shown), the globules were reduced to remnants with indistinct edges and heights of 1 to 3 nm instead of the typical globular height of about 10 to 15 nm on control foliar surfaces.

The effect of NaOCl treatment on the foliar globules as viewed by AFM is shown in Figures 8 and 9. After 1 day, the globules remained relatively intact. By 5 days, the globules were blurred and reduced in height to a range of 3 to 8 nm. In both the NaOH and NaOCl treatments, the surfaces became smoother and relatively featureless with time.

Treatment of foliar chips for 48 h with the proteolytic enzymes (carboxypeptidase B, endoproteinase glu-C, and subtilisin) also led to the partial removal of the foliar globules. In each case, as illustrated for carboxypeptidase B (Figs. 10 and 11), the globules became indistinct and reduced in height relative to control globules.

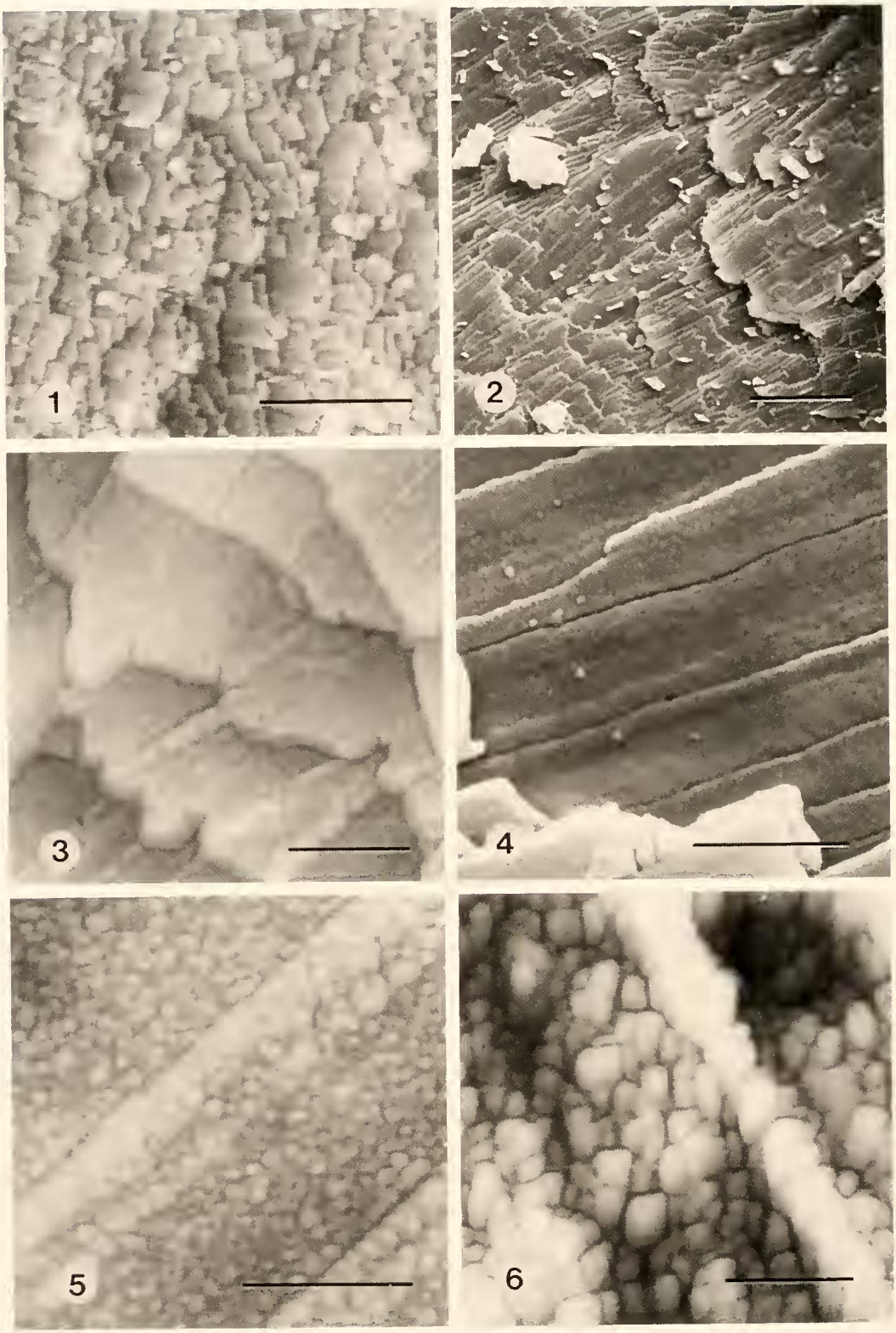

Figures 1–6. Micrographs of untreated (control) chips of oyster shell folia.

The surfaces of foliar chips that had been treated with the antibody to the oyster shell protein were coated with globular material as seen by AFM (Figs. 12 and 13). These globules of immunoglobulins were 4 to 5 times as large as the untreated foliar globules (compare Figs. 6 and 13).

AFM and SEM images of a foliar chip on which calcite crystals were grown can be compared (Figs. 14–16). In both types of micrographs, the newly formed crystals appeared to be very smooth and to emerge from the foliar surface at an oblique angle. Because these ectopic crystals were not coated with protein, the atomic pattern of the lattice surface could be resolved by AFM (Fig. 17).

The spacings and angles between the positions of hundreds of atoms of the surface of crystal growth were measured directly on several images by manual placement of the cursor onscreen and use of the measurement tools of the software. In addition, Fourier analysis was applied to the average periodicities of the entire images. The AFM software readily supplies measurements by both of these approaches.

The measured atomic spatial relationships were then compared to the theoretical spatial relationships generated by computer models of various possible surfaces of calcite (Cerius^2, molecular modeling software, Molecular Simulations, Inc.). A similar approach has been helpful in identifying other calcite surfaces such as the (104) cleavage surface of control calcite rhombohedrons and the (001) basal plane of calcite nucleated on glass (Sikes *et al.*, 1994), as well as the (1 −1 0) surface of calcite crystals that were stabilized by the presence of polyaspartate (Sikes and Wierzbicki, 1996).

The first identifiable surface of the ectopic foliar crystals appeared to be the (1 −1 0) plane of calcite. The AFM atomic image (Fig. 17) was compared to a computer model of the (1 −1 0) surface (Fig. 18). The measured spacings and angles between the various atomic positions matched within 5% of the theoretical values in all cases, as explained in the legend of Figure 18.

Discussion

The results supported the identity of the foliar globules, at least in part, as molecules of oyster shell protein, rather than only mineral material. That is, the globules exhibited (1) slow dissolution in NaOH and NaOCl, (2) reactivity to an antibody specific to oyster shell protein, (3) partial hydrolysis by proteolytic enzymes, and (4) morphological similarity to ellipsoids and globules of isolated protein from oyster shell as observed in prior studies.

The correspondence in size and appearance between the foliar globules and the isolated molecules of the protein was evident in AFM images that were prepared in a variety of ways. For example, the isolated protein was bound to calcite and viewed by AFM both in fluids and on rinsed, then dried crystals. The protein exhibited ellipsoid and globular morphologies with lengths and widths in the range of 50 to 100 nm, similar to those of the foliar globules (Donachy *et al.*, 1992; Wierzbicki *et al.*, 1994; Sikes *et al.*, 1994). The isolated protein also exhibited comparable morphologies when viewed either bound on glass and mica in fluids or when dried onto these substrates (Sikes and Wierzbicki, 1995a, b; 1996; Sikes *et al.*, 1997).

The protein used in the prior studies was obtained as a distinct, reversed-phase peak from the EDTA-soluble, proteinaceous matrix of the shells (Wheeler *et al.*, 1988; Wheeler and Sikes, 1989; Rusenko *et al.*, 1991). The peak is polydisperse, with an estimated gel-permeation molecular mass of approximately 50 kD. The protein is anionic with about 30% of the residues being aspartate and nearly 30% being serine, much of which is phosphorylated.

If the foliar globules are proteinaceous in part, they would of necessity seem to be agglomerations. That is, the AFM volume ($4/3\ \pi\ abc$) of the foliar globular ellipsoids of about 100 nm length (a = 50 nm), 50 nm width (b = 25 nm), and 10 nm height (c = 5 nm) is 2.62×10^{-17} cm^3. The theoretical molecular volume ($4/3\ \pi\ r^3$) of a globular protein of the size of a typical soluble oyster shell protein (M_w 50 kD, diameter ~5.4 nm; Cantor and Schimmel, 1980) is about 8.24×10^{-20} cm^3. Comparison of these values, assuming for the moment that the globules are entirely protein, yields an estimate of about 318 molecules of oyster shell protein per globule. Lower estimates would result if larger proteins of the shell matrix were

Figure 1. Atomic force micrograph of a dry, untreated chip. Range of lath heights: 150–350 nm. Scale bar = 15 μm.

Figure 2. Scanning electron micrograph of an untreated chip. Scale bar = 25 μm.

Figure 3. Atomic force micrograph of a dry, untreated chip. Range of lath heights: 150–250 nm. Scale bar = 2 μm.

Figure 4. Scanning electron micrograph of an untreated chip. Scale bar = 2 μm.

Figure 5. Atomic force micrograph of a dry, untreated chip. Total range of elevation within the imaged area = 70 nm. Scale bar = 1 μm.

Figure 6. Atomic force micrograph of a dry, untreated chip. Typical globular height = 10 to 15 nm; maximum globular height in the imaged area = 40 nm. Scale bar = 250 nm.

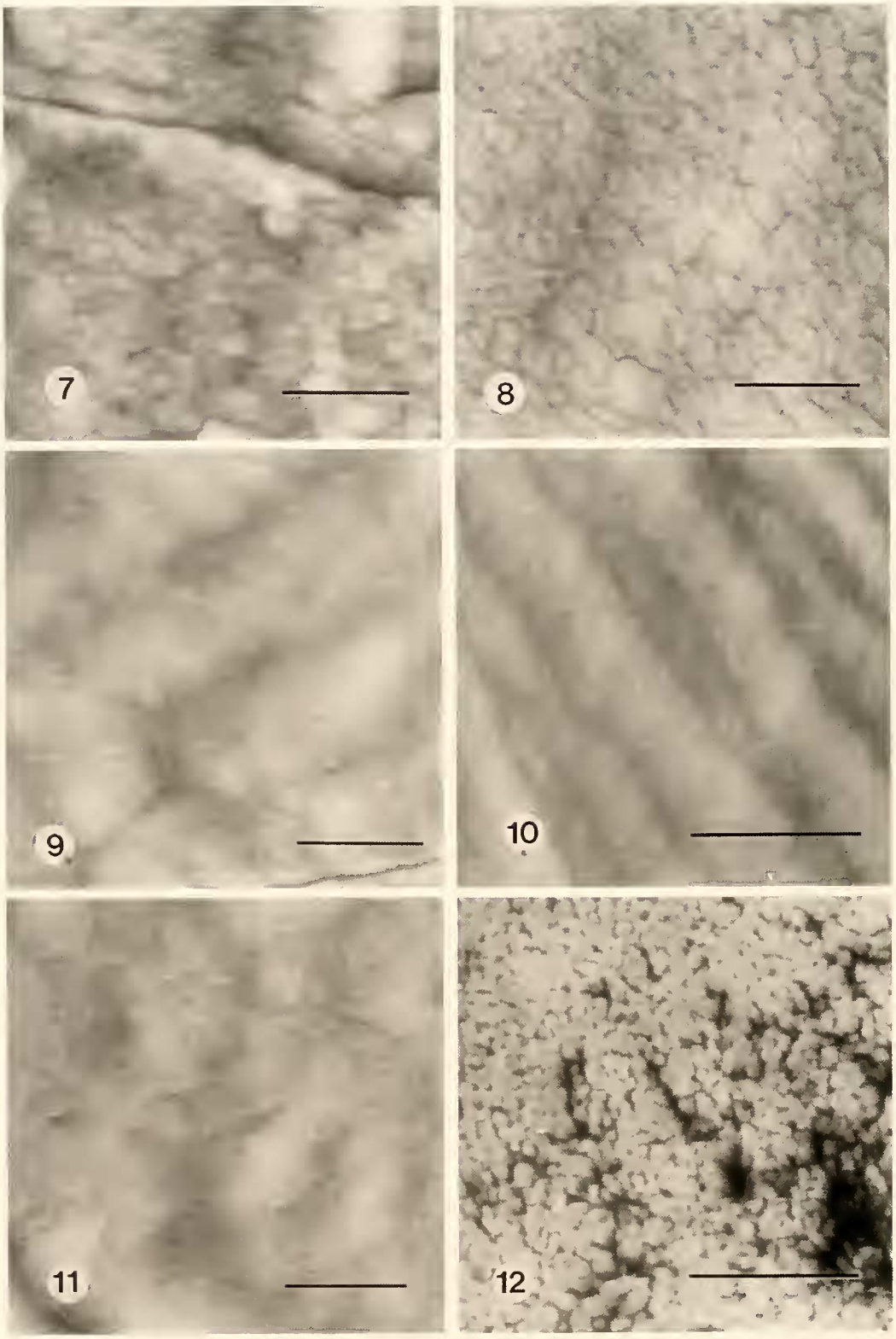

Figures 7–12. Atomic force micrographs of dry chips of oyster shell folia treated with various substances.

considered. For example, the proteins from oyster shell exhibit a continuum of molecular weights that ranges into the millions for soluble fractions. Also present are insoluble fractions with an amino acid composition similar to that of the soluble proteins (Wheeler *et al.*, 1988).

Phosphoproteins similar to the oyster shell protein are known to form micellar agglomerations in solution. For example, Marsh (1989a, b) reviewed the associative behavior of casein and other phosphoproteins and demonstrated that the phosphophoryn from tooth dentin forms agglomerations that are held together *via* ionic interactions with cations such as calcium and magnesium. Phosphophoryn, which—like the oyster shell protein—is highly enriched in phosphoserine and aspartic acid, formed particles of about 25 nm in diameter that contained perhaps 75 monomers per particle.

AFM and TEM observations by Fincham *et al.* (1994, 1995) of 15–20 nm "nanospheres" on the calcium phosphate surfaces of developing enamel have also been interpreted as proteinaceous, composed of amelogenin proteins. The amelogenins are smaller (~20 kD) and more hydrophobic than the typical oyster shell protein. The amelogenic nanospheres are thought to be agglomerations of greater than 100 monomers.

Globular ellipsoids in the range of 100 nm have also been observed on the surfaces of $CaCO_3$ otoconia from the inner ear of a newt (Hallworth *et al.*, 1995). The otoconia were isolated intact and are known to have associated proteins. Observed with AMF, the otoconial surface globules were quite like the foliar globules in appearance and were attributed to crystal formation as mediated by the otoconial proteins.

Our results indicate that the foliar globules are probably not composed solely of protein. The comparative images revealed that the foliar globules were generally taller at 10 to 40 nm than the ellipsoids and globules of isolated protein on calcite, mica, and glass, which had heights generally in the range of a few nanometers. Furthermore, the foliar globules resisted dissolution in NaOCl and NaOH. Mutvei (1977, 1978) also reported the presence of hypochlorite-resistant, "calcified" organic matrices associated with the surfaces of nacreous tablets of molluscan shell, and Towe (1990) commented on the resistance to household bleach of some matrix-like organic molecules, particularly if they were intimately associated with the mineral. Thus it seems that, in addition to protein, the foliar globules may contain a phase of mineral salts and perhaps water, as discussed below.

One assignment of the relative amounts of the mineral and organic phases of shell can be made by quantifying the weight of each component. Another assignment can be made by comparing the volumes of each layer, taken from the linear dimensions of each phase as seen in both SEM and AFM images, correcting for density differences of the mineral and the proteinaceous material. The observed linear dimensions as determined by SEM and AFM, although subject to different kinds of artifacts, were in agreement, lending credence to the estimates.

The protein content of oyster shell has been variously measured as ranging from perhaps a few tenths of 1% to no more than 3% by weight in whole shells (Korringa, 1951; Weiner and Hood, 1975; Price *et al.*, 1976; Rusenko, 1988; Rusenko *et al.*, 1991), with the protein content of the foliar layers alone placed at $<1\%$. A lower protein content for foliar layers is consistent with the electron microscopic observations, all of which revealed that the foliar layer lacks the thicker, "interlamellar" organic layer of the prismatic regions of shell.

Given this range of values reported for protein content, an analysis of the apparent, relative volumes of "nonmineral" and mineral layers in a foliar lath as seen in both electron micrographs and atomic force micrographs yields an estimate of nonmineral content that is too high to be attributable only to organic matter. For example, Watabe and Wilbur (1961) and Watabe (1965) in electron microscopic studies observed the laths to be composed of crystal blocks that were surrounded by "intercrystalline" organic material. The dimensions of each block ranged from 10 to 40 nm in width, 15 to 200 nm in height, and ~4 μm in length. The dimensions of the organic matrix ranged

Figure 7. Treatment: 1 *N* NaOH for 5 days. Total range of elevation within the imaged area = 80 nm; range of globular heights = 4 to 30 nm. Scale bar = 500 nm.

Figure 8. Treatment: 5.25% NaOCl for 24 hours. Total range of elevation within the imaged area = 18 nm; heights of globular remnants = 3 to 6 nm. Scale bar = 250 nm.

Figure 9. Treatment: 5.25% NaOCl for 5 days. Total range of elevation within the imaged area = 16 nm; heights of globular remnants = 2 to 4 nm. Scale bar = 250 nm.

Figure 10. Treatment: Carboxypeptidase B for 48 hours. Total range of elevation within the imaged area = 30 nm, heights of globular remnants = 3 to 5 nm. Scale bar = 1 μm.

Figure 11. Treatment: Carboxypeptidase B for 48 hours. Total range of elevation within the imaged area = 15 nm. Scale bar = 250 nm.

Figure 12. Treatment: An antibody to the isolated oyster shell protein. Foliar laths are obscured by copiously bound antibody molecules. Scale bar = 5 μm.

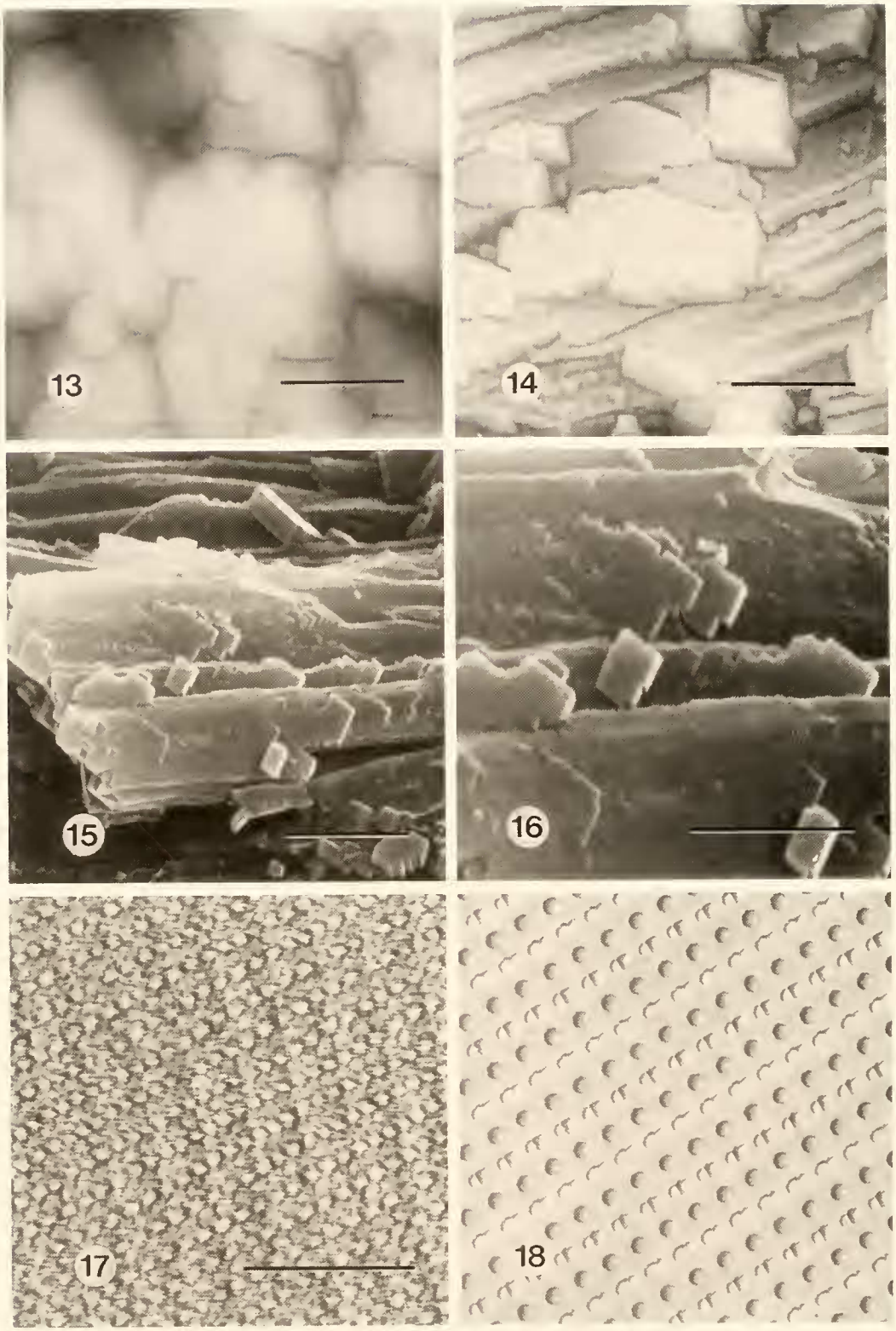

Figures 13–18

from 12 nm to 20 nm, as also later recorded by Taylor *et al.* (1969). These values for the dimensions both of the crystal blocks and of the organic layers are similar to the dimensions of the crystal laths and the foliar globules observed by AFM and recorded herein.

Based on average values of these dimensions and a simple calculation of the volume of the crystal block and the volume of the encapsulating proteinaceous layer, corrected for the density of calcite (2.71; Weast *et al.*, 1988) and typical proteins (~1.35; White *et al.*, 1973), the protein content would be about 17% by weight, which of course is too high. A plausible explanation for the high estimate is that the foliar globules seen with AFM and the organic layer seen in electron micrographs might consist of both protein and mineral, with the latter filling in spaces around and between the molecules of protein.

Another possible complication is that actual volumes of the foliar globules and the AFM volumes might be different, as sometimes occurs in AFM studies. The discrepancy is most likely to reflect an overestimate of the length and width of molecules. This kind of tip artifact results when the inverted pyramidal AFM tip slides up and down the sides of objects that are actually sharp, giving a smoothed and widened appearance (Hansma *et al.*, 1995; Giles *et al.*, 1994, 1995) and perhaps exaggerating the length or width by about 20%.

This convolution phenomenon is not a simple function and does not always occur: as demonstrated by the comparison of the micrographs produced by SEM and AFM, AFM showed true foliar morphology. Similarly, AFM micrographs of peptides bound to calcite (Wierzbicki *et al.*, 1994; Sikes *et al.*, 1993, 1994, 1997) and of various other molecules bound to flat substrates—for example, DNA to mica (Hansma and Hoh, 1994; Hansma *et al.*, 1995)—revealed molecular morphologies that were consistent with theory.

The height measurements at the top of an elevation, particularly of firm surfaces such as the foliar globules, are considered to be generally reliable, depending on the method of standardization. We calibrate our scanners at the micrometer level by use of commercial standards (Digital Instruments) and at the angstrom level by use of well-characterized crystals such as mica for the x and y axes, and calcite [the step height of the cleavage surface (104)] for the z axis.

Overall, the results and analysis suggest that the foliar globules are composed in significant part of protein. An undefined mineral phase that fills in the spaces around and within the foliar globules also may be a significant component, along with water, gases, and other mineral salts as minor components. In fact, Galtsoff (1964) viewed initiation of oyster shell growth as crystallization

---

Figure 13. Atomic force micrograph of a dry chip of oyster shell folia that was treated with an antibody to the isolated oyster shell protein. Total range of elevation within the imaged area = 150 nm (compare to Fig. 6, a control chip at the same magnification). Scale bar = 250 nm.

Figure 14. Atomic force micrograph of calcite crystals that were nucleated on an untreated chip of oyster shell folia at 10 m*M* Ca^{2+}, 7 m*M* inorganic carbon, initial pH 8.3, in artificial seawater (imaged in this fluid). Height of the central ectopic crystal = 340 nm, with a plane angle $<10°$ between the crystal surface and the underlying foliar surfaces. Scale bar = 2.5 μm.

Figure 15. Scanning electron micrograph of calcite crystals that were nucleated on the oyster shell foliar surface of Figure 14. Scale bar = 3 μm.

Figure 16. Scanning electron micrograph of calcite crystals that were nucleated on the oyster shell foliar surface of Figure 14. Scale bar = 2 μm.

Figure 17. Atomic force micrograph of the lattice atoms of the surface of the central crystal of Figure 14, imaged in fluid as above. Total range of elevation within the imaged area = 3 Å. Scale bar = 5 nm.

Figure 18. Computer diagram of the (1 −1 0) surface of calcite showing calcium atoms (grey) and carbonate groups (with white oxygens) in alternating rows. The spacing between lattice positions in the rows (diagonal upward, left to right) of both calcium atoms and carbonate groups is 4.99 Å. The spacing between lattice positions perpendicular to the rows (that is, between a calcium atom and the nearest oxygen of an adjacent carbonate group) is 4.265 Å. Both of these distances matched the spacings observed in the AFM of Figure 17. The computer model showed that an oxygen of each carbonate group is elevated ~1 Å relative to the plane of calcium atoms, and therefore the most distinct and separate atoms of Figure 17 are thought to be oxygen atoms. The specific carbonate oxygens that are most protuberant in each row differ in alternating rows, creating a slight zig-zag pattern (the oxygens of alternating rows do not line up exactly along the diagonal from upper left to lower right). This is visible in both the image of Figure 17 and the model. Similarly, the lower atoms were measured in Figure 17 to be in agreement with theory at ~1 Å below the plane of the higher atoms, and thus are thought to be calcium atoms that blended together somewhat in the image, probably owing to the interaction between the AFM tip and the lattice during imaging in the troughs. The agreement between these and other features of the experimental image (Fig. 17) and the theoretical model (Fig. 18) lead to the assignment of the surface of the crystal as most likely the (1 −1 0) surface of calcite.

within a gelatinous organic secretion of the mantle, with the mineral imbedded within the matrix of organic matter (see also Carriker *et al.,* 1980; Crenshaw, 1990).

Certainly, an important function of the oyster shell protein might be to nucleate calcite from the extrapallial fluid, which would be supersaturated during shell formation. However, the foliar globules were not particularly effective as crystal nucleators. That is, under metastable conditions in the AFM assay at 2 to 5 m*M* DIC, which readily supported growth of calcite seeds, there was no crystal growth associated with the globules. Furthermore, under the metastable conditions, exposed regions of mineral on fracture surfaces at the sides or ends of laths did exhibit crystal growth when the organic-coated foliar surfaces did not. Even after 2 h at 5 m*M* DIC when crystals had spontaneously nucleated and could be seen flowing past the probe during scanning, (via the top-view videomicroscopy capability of the AFM system) crystal growth was not observed in association with the foliar globules.

It seems clear that a preexisting mineral phase would be the best nucleator for further lattice formation of that phase. In an AFM study of bivalve shell, Giles *et al.* (1995) noted that aragonite growth of the molluscan nacreous layer could have been nucleated by small regions of uncoated mineral on nacreous tablets. Watabe (1981) and later Manne *et al.* (1994) had previously offered this as a mechanism for continued nucleation during growth of nacre. In summary, it may be that the issue is not so much the nucleation of calcite on the foliar surface, but rather exactly how the foliar morphology is continually sustained layer-upon-layer during growth of the shell.

If the nucleation of a new layer of calcite occurs on exposed regions of calcite, the lack of ready nucleation on the foliar surfaces suggests either that the putative mineral phase of the foliar globules was not exposed to the metastable fluid or that, if exposed, the mineral phase is not crystalline calcite. An analogous arrangement of phosphoproteins and a mineral phase has been observed in some molluscs. For example, agglomerations of phosphoproteins and mineral salts (sometimes an amorphous calcium phosphate phase) of about 40-nm diameter have been reported as part of a nonmineralizing, organic lamella that contacts the shells of some molluscs (Marsh and Sass, 1983, 1984). These particles also occur in the fluids that bathe the shell in some molluscs, but they were not observed in the American oyster (Marsh and Sass, 1985). Again, neither these globules nor the aforementioned agglomerations of dentin phosphophoryn, which also are thought to contain an amorphous mineral phase, seemed to act as nucleators of the crystalline mineral phase of shell or teeth (Marsh, 1986, 1989a, b, 1994).

The crystallographic identity of the foliar surface of oyster shell has been studied by several authors with different results. For example, on the basis of X-ray data, Wada (1963, 1968) and Watabe (1965, 1981) assigned the foliar surfaces as the basal plane (001), with the sides probably hexagonal planes, essentially similar to the crystallographic arrangement of molluscan prismatic nacre. In this case, the *c*-axis would be perpendicular to the foliar surface, with the hexagonal planes parallel to the *c*-axis. The oyster shell protein is thought to have high affinity for each of these surfaces (Sikes *et al.*, 1993, 1994; Sikes and Wierzbicki, 1995a, b, 1996; Wierzbicki *et al.*, 1994, including references to other workers).

In contrast, Taylor *et al.* (1969) used optical measurements and X-ray patterns to suggest that the plane of foliation was not (001) and that the *c*-axis was inclined to the foliar plane at a shallow angle (26° in *Placuna placenta*). These authors also theorized that there may, in fact, be no definable crystallographic plane of initial foliation of each layer in that the foliar crystals are not planar on top when viewed in both surface and cross-sectional electron micrographs. Giles *et al.* (1995) further considered the rounded globules of hypochlorite-treated nacre as inorganic, aragonite surfaces that possibly consisted of many steps at the nanoscale, thus suggesting a complex mechanism of crystal growth.

Runnegar (1984) also made extensive X-ray and optical assessments of the crystallography of foliar layers from various bivalves, including *C. virginica.* From these studies, he noted an inclination of the *c*-axis relative to the foliar plane. Using scanning electron micrographs and aluminum models of calcite rhombohedrons ectopically grown from hypochlorite-treated foliar chips, he further demonstrated this inclination by the tilted appearance of the crystals and models relative to the foliar surface. The oyster shells of his study exhibited folia with more than one type of inclination of the *c*-axis, even within a single shell. Runnegar acknowledged that the reports of (001) foliar surfaces in some specimens by other workers also seemed to be correct, although he did not observe this arrangement.

Our observations of calcite crystals grown on untreated chips of oyster shell folia at 7 m*M* DIC in the AFM assay support the findings of both Taylor *et al.* (1969) and Runnegar (1984). Even the early stages of crystal formation often exhibited an inclination of the ectopic crystals relative to the foliar surface. The (1 −1 0) plane of calcite appeared as a principal surface identifiable by AFM during the early growth of the crystals. This plane is parallel to the *c*-axis, and therefore its angle of inclination is the same as that of the *c*-axis. By use of the plane-angle function of the AFM imaging software, which is designed for first designating planes of interest and then calculating the angles between them, angles between the foliar plane and the ectopic crystal surfaces were measured. In a few

cases, angles close to 64° (Runnegar's type 3 arrangement) were observed. However, much shallower angles were frequently seen as well.

The (1 −1 0) surface of calcite is one of several surfaces that are likely to be expressed during ectopic crystal growth, particularly at the higher of the supersaturations used herein, which actually were significantly lower than those of Runnegar (1984). Although crystals did not appear to nucleate on the foliar globules at our lower supersaturations (≤5 m*M* DIC), the higher supersaturations (≥7 m*M* DIC) did result in rapid and widespread crystal growth on the foliar surfaces. Even so, the precise site of nucleation was not easily discernible because the ectopic crystals usually spanned more than one lath, as well as the sides of laths. The exact spatial and crystallographic relationships, if any, between the foliar globules and calcite nucleation will require further study under controlled conditions of metastable supersaturation that reflect conditions *in vivo*.

Acknowledgments

This work was supported by grants EHR-9108761 from the National Science Foundation, C-3662 from the Research Corporation, and R/MX-6 from the South Carolina Sea Grant Consortium.

Literature Cited

Cantor, C. R., and P. R. Schimmel. 1980. *Biophysical Biochemistry. Part I. The Conformation of Biological Molecules.* W. H. Freeman, San Francisco.

Carriker, M. R., and R. E. Palmer. 1979. Ultrastructural morphogenesis of prodissoconch and early dissoconch valves of the oyster *Crassostrea virginica*. *Proc. Natl. Shellfish. Assoc.* **69:** 103–128.

Carriker, M. R., R. E. Palmer, and R. S. Prezant. 1980. Functional ultramorphology of the dissoconch valves of the oyster *Crassostrea virginica*. *Proc. Natl. Shellfish. Assoc.* **70:** 139–183.

Crenshaw, M. A. 1990. Biomineralization mechanisms. Pp. 1–9 in *Skeletal Biomineralization: Patterns, Processes, and Evolutionary Trends. Volume I.* J. G. Carter, ed. Van Nostrand Reinhold, New York.

Donachy, J. E., B. Drake, and C. S. Sikes. 1992. Sequence analysis and atomic force microscopy of a matrix protein from the shell of the oyster *Crassostrea virginica*. *Mar. Biol.* **114:** 423–428.

Drake, B., R. Hellmann, C. S. Sikes, and M. L. Ocelli. 1992. Atomic scale imaging of albite feldspar, calcium carbonate, rectorite, and bentonite using atomic force microscopy. *SPIE Proc.* **1639:** 151–159.

Fincham, A. G., J. Moradian-Oldak, J. P. Simmer, P. Sarte, E. C. Lau, T. Diekwisch, and H. C. Slavkin. 1994. Self-assembly of a recombinant amelogenin protein generates supramolecular structures. *J. Struct. Biol.* **112:** 103–109.

Fincham, A. G., J. Moradian-Oldak, and H. C. Slavkin. 1995. Evidence for amelogenin "nanospheres" as functional components of secretory-stage enamel matrix. *J. Struct. Biol.* **115:** 50–59.

Friedbacher, G., P. K. Hansma, E. Ramli, and G. D. Stucky. 1991. Imaging powders with the atomic force microscope: from biominerals to commercial materials. *Science* **253:** 1261–1263.

Galtsoff, P. S. 1964. The American oyster *Crassostrea virginica* Gmelin. *Fish. Bull.* **64:** 1–480.

Giles, R., S. Manne, C. M. Zaremba, A. Belcher, S. Mann, D. E. Morse, G. D. Stucky, and P. K. Hansma. 1994. Imaging single nacreous tablets with the atomic force microscope. *Mater. Res. Soc. Symp. Proc.* **332:** 413–422.

Giles, R., S. Manne, S. Mann, D. E. Morse, G. D. Stucky, and P. K. Hansma. 1995. Inorganic overgrowth of aragonite on molluscan nacre examined by atomic force microscopy. *Biol. Bull.* **188:** 8–15.

Gutmannshauer, W., and H. A. Hänni. 1994. Structural and chemical investigations on shells and pearls of nacre forming salt- and fresh-water bivalve molluscs. *J. Gemmology* **24:** 241–252.

Hallworth, R., M. L. Wiederhold, J. B. Camphell, and P. S. Steyger. 1995. Atomic force microscope observations of otoconia in the newt. *Hear. Res.* **85:** 115–121.

Hansma, H. G., and J. H. Hoh. 1994. Biomolecular imaging with the atomic force microscope. *Annu. Rev. Biophys. Biomol. Struct.* **23:** 115–139.

Hansma, H. G., D. E. Laney, M. Bezanilla, R. L. Sinsheimer, and P. K. Hansma. 1995. Applications for atomic force microscopy of DNA. *Biophys. J.* **68:** 1672–1677.

Hilner, P. E., A. J. Gratz, S. Manne, and P. K. Hansma. 1992. Atomic scale imaging of calcite growth and dissolution in real time. *Geology* **20:** 359–362.

Korringa, P. 1951. On the nature and function of "chalky" deposits in the shell of *Ostrea edulis* Linnaeus. *Proc. Calif. Acad. Sci.* **27:** 133–158.

Kuhn-Spearing, L. T., H. Kessler, and S. M. Spearing. 1996. Fracture mechanisms of the *Strombus gigas* conch shell: implications for design of brittle laminates. *J. Mater. Sci.* **31:** 6583.

Mann, S. (ed.). 1996. *Biomimetic Approaches in Materials Science,* VCH Publishers, New York.

Manne, S., C. M. Zaremba, R. Giles, L. Huggins, D. A. Walters, A. Belcher, D. E. Morse, G. D. Stucky, J. M. Didymus, S. Mann, and P. K. Hansma. 1994. Atomic force microscopy of the nacreous layer in mollusc shells. *Proc. R. Soc. Lond. B Biol. Sci.* **256:** 17–23.

Marsh, M. E. 1986. Biomineralization in the presence of calcium-binding phosphoprotein particles. *J. Exp. Zool.* **239:** 207–220.

Marsh, M. E. 1989a. Self-association of calcium and magnesium complexes of dentin phosphophoryn. *Biochemistry* **28:** 339–345.

Marsh, M. E. 1989b. Binding of calcium and phosphate ions to dentin phosphophoryn. *Biochemistry* **28:** 346–352.

Marsh, M. E. 1994. Polyanions and biomineralization. *Bull. Inst. Oceanogr. (Monaco)* **14(1):** 121–128.

Marsh, M. E., and R. L. Sass. 1983. Calcium-binding phosphoprotein particles in the extrapallial fluid and innermost shell lamella of clams. *J. Exp. Zool.* **226:** 193–203.

Marsh, M. E., and R. L. Sass. 1984. Phosphoprotein particles: calcium and inorganic phosphate binding structures. *Biochemistry* **23:** 1448–1456.

Marsh, M. E., and R. L. Sass. 1985. Distribution and characterization of mineral-binding phosphoprotein particles in bivalvia. *J. Exp. Zool.* **234:** 237–242.

Mohammed, H. D., R. Yamamoto, T. E. Carpenter, and H. B. Ortmayer. 1986. A statistical model to optimize enzyme-linked immunosorbent assay parameters for detection of *M. gallisepticum* and *M. synoviae* antibodies in egg yolk. *Avian Dis.* **30:** 389–397.

Mutvei, H. 1977. The nacreous layer in *Mytilus, Nucula,* and *Unio* (Bivalvia). *Calcif. Tissue Res.* **24:** 11–18.

Mutvei, H. 1978. Ultrastructural characteristics of the nacre in some gastropods. *Zool. Scr.* **7:** 287–296.

Myers, J. M., A. Veis, B. Sahsay, and A. P. Wheeler. 1996. A

method for enhancing the sensitivity and stability of stains-all for phosphoproteins separated in sodium dodecyl sulfate-polyacrylamide gels. *Anal. Biochem.* **240:** 300–302.

Price, T. J., G. W. Thayer, M. W. LaCroix, and G. P. Montgomery, 1976. The organic content of shells and soft tissues of selected estuarine gastropods and pelecypods. *Proc. Natl. Shellfish. Assoc.* **65:** 26–31.

Runnegar, B. 1984. Crystallography of the foliated calcite shell layers of bivalve molluscs. *Alcheringa* **8:** 273–290.

Rusenko, K. W. 1988. Studies on the structure and function of shell matrix proteins from the American oyster, *Crassostrea virginica*. Ph.D. Dissertation, Clemson University, Clemson, SC. 287 pp.

Rusenko, K. W., J. E. Donachy, and A. P. Wheeler, 1991. Purification and characterization of a shell matrix phosphoprotein from the American oyster. Pp. 107–124 in *Surface Reactive Peptides and Polymers: Discovery and Commercialization,* C. S. Sikes and A. P. Wheeler, eds. ACS Symposium Series 444. ACS Books, Washington, DC.

Sikes, C. S., and A. Wierzbicki. 1995a. Mechanisms of regulation of crystal growth in selected biological systems. Pp. 183–206 in *Mineral Scale Formation and Inhibition,* Z. Amjad, ed. Plenum Press, New York.

Sikes, C. S., and A. Wierzbicki. 1995b. Atomic force microscopy and molecular modeling of protein bound to calcite. *SPIE Proc.* **2547:** 164–174.

Sikes, C. S., and A. Wierzbicki. 1996. Polyamino acids as antiscalants, dispersants, antifreezes, and absorbent gelling materials. Pp. 249–278 in *Biomimetic Approaches in Materials Science,* S. Mann, ed. VCH Publishers, New York.

Sikes, C. S., E. Mueller, J. D. Madura, B. Drake, and B. J. Little. 1993. Polyamino acids as antiscalants, corrosion inhibitors, and dispersants: atomic force microscopy and mechanisms of action. *Corrosion 93,* paper **465:** 1–21.

Sikes, C. S., A. Wierzbicki, and V. Fabry. 1994. From atomic to global scales in biomineralization. *Bull. Inst. Oceanogr. (Monaco)* **14(1):** 1–49.

Sikes, C. S., F. Martin, A. Wierzbicki, and A. P. Wheeler. 1997. Atomic force microscopy and enzymatic degradation of oyster shell protein and polyaspartate. *Macromol. Symp.* **123:** 85–92.

Stupp, S. I., and P. V. Braun. 1997. Molecular manipulation of microstructures: biomaterials, ceramics, and semiconductors. *Science* **277:** 1242–1248.

Taylor, J. D., W. J. Kennedy, and A. Hall. 1969. The shell structure and mineralogy of the bivalvia. Introduction. Nuculacea-Trigonacea. *Bull. Br. Mus. (Nat. Hist.) Zool., Supplement* **3:** 1–125, plates 1–29.

Towe, K. M. 1990. Overviews of biomineralization. *Paleobiology* **16:** 521–526.

Wada, K. 1963. Studies on the mineralization of the calcified tissue in molluscs. VI. Crystal structure of the calcite grown on the inner surface of calcitostracum. *J. Electron Microsc.* **12:** 224–227.

Wada, K. 1968. Spiral growth of calcitostracum. *Nature* **219:** 62.

Watabe, N. 1965. Studies on shell formation. XI. Crystal-matrix relationships in the inner layers of mollusk shells. *J. Ultrastruct. Res.* **12:** 351–370.

Watabe, N. 1981. Crystal growth of calcium carbonate in the invertebrates. *Prog. Crystal Growth Charact.* **4:** 99–147.

Watabe, N., and K. M. Wilbur. 1961. Studies on shell formation. IX. An electron microscope study of crystal layer formation in the oyster. *J. Biophys. Biochem. Cytol.* **9:** 761–771.

Watabe, N., D. G. Sharp, and K. M. Wilbur. 1958. Studies on shell formation. VIII. Electron microscopy of crystal growth of the nacreous layer of the oyster *Crassostrea virginica*. *J. Biophys. Biochem. Cytol.* **4:** 281–284, plates 152–156.

Weast, R. C., M. J. Astle, and W. H. Beyer (eds.). 1988. *CRC Handbook of Chemistry and Physics,* CRC Press, Boca Raton, FL.

Weiner, S., and L. Addadi. 1997. Design strategies in mineralized biological materials. *J. Mater. Chem.* **7:** 689–702.

Weiner, S., and L. Hood. 1975. Soluble protein of the organic matrix of mollusk shells: a potential template for shell formation. *Science* **190:** 987–989.

Wheeler, A. P., and L. P. Koskan. 1993. Large scale thermally synthesized polyaspartate as a biodegradable substitute in polymer applications. *Mater. Res. Soc. Symp. Proc.* **292:** 277–283.

Wheeler, A. P., and C. S. Sikes. 1989. Matrix-crystal interactions in $CaCO_3$ biomineralization. Pp. 95–133 in *Biomineralization: Chemical and Biochemical Perspectives,* S. Mann, J. Webb, and R. J. P. Williams, eds. VCH Publishers: Weinheim, FRG.

Wheeler, A. P., K. W. Rusenko, D. M. Swift, and C. S. Sikes. 1988. Regulation of $CaCO_3$ formation by fractions of oyster shell matrix. *Mar. Biol.* **98:** 71–80.

Wheeler, A. P., K. C. Low, and C. S. Sikes. 1991. $CaCO_3$ crystal-binding properties of peptides and their influence on crystal growth. Pp. 72–84 in *Surface Reactive Peptides and Polymers: Discovery and Commercialization,* C. S. Sikes and A. P. Wheeler, eds. ACS Symposium Series 444. ACS Books, Washington, DC.

White, A., P. Handler, and E. L. Smith. 1973. *Principles of Biochemistry,* McGraw Hill, New York.

Wierzbicki, A., C. S. Sikes, B. Drake, and J. Madura. 1994. Atomic force microscopy and molecular modeling of protein and peptide binding to calcite. *Calcif. Tissue Int.* **54:** 133–141.